A Biologically Inspired Sensor Mechanism for Amplification of Tactile Signals Based on Parametric Resonance

T. Volkova, I. Zeidis and K. Zimmermann

Abstract In this paper, the vibrational motion of an elastic beam under the parametric excitation is investigated theoretically and numerically. The problem is motivated by biological tactile sensors, called vibrissae or whiskers. Mammals use these thin long hairs for exploration of the surrounding area, object localization and texture discrimination. We propose a mechanical model of the vibrissa sweeping across a rough surface as a straight truncated beam stimulated by a periodic following force. The equation of transverse motion of the beam is studied using the Euler–Bernoulli beam theory and asymptotic methods of mechanics. The numerical analysis is performed by means of the finite element method. It is shown that the parametric resonance of the beam occurs at the specific ranges of the excitation frequency, which depend on the parameters of the beam and the amplitude of the applied force. For these frequency values, the vibrations of the beam are unstable with exponentially increasing amplitude. The comparison of the resonance ranges obtained theoretically and numerically is made. Thus, together with the realisation of the viscoelastic support of an artificial tactile sensor, the parametric resonance may be a potentially useful method for amplifying small signals arising from the contact with an object.

Keywords Parametric resonance · Vibration · Beam theory · Method of averaging · Vibrissa

T. Volkova · I. Zeidis (✉) · K. Zimmermann
Technical Mechanics Group, Department of Mechanical Engineering,
Technische Universität Ilmenau, Ilmenau, Germany
e-mail: igor.zeidis@tu-ilmenau.de

T. Volkova
e-mail: tatiana.volkova@tu-ilmenau.de

K. Zimmermann
e-mail: klaus.zimmermann@tu-ilmenau.de

L. Zentner et al. (eds.), *Microactuators and Micromechanisms*,
Mechanisms and Machine Science 45, DOI 10.1007/978-3-319-45387-3_3

1 Introduction

In nature, all mammals except humans possess specialised tactile hairs, called *vibrissae* or *whiskers*. These thin long hairs grow usually in groups in different locations on an animal's body. Among the most familiar to us are *mystacial* vibrissae orderly distributed over the whiskerpad on a muzzle, *supraorbital* vibrissae above the eyes, and *carpal* vibrissae that are located on the downside aspect of the forelimbs (Fig. 1). For terrestrial and marine mammals, vibrissae are significantly important tactile sensors used for the exploration of the surrounding area, texture discrimination, or even detection of water vibrations (Dehnhardt and Kaminski 1995; Niederschuh et al. 2014; Vincent 1912).

The structure and characteristics of vibrissae differ considerably from normal body hairs of the same mammal individual. They are thicker and stiffer than other types of hairs and have a conical shape with the linearly decreasing diameter (Voges et al. 2012). Another significant difference lies in the more complicated base of the vibrissa. The vibrissal hair grows from a special follicle, called the *follicle-sinus complex* (FSC). It incorporates lots of sensory nerve endings and a capsule of blood (Ebara et al. 2002). For some groups of vibrissae, the FSC is surrounded by two types of muscles that allow an animal to move its vibrissae back and forth (Dörfl 1982). These sniffing active movements of vibrissae, called *whisking*, play an important role during the exploratory behaviour of mammals.

The fascinating biological paradigm of the vibrissal tactile sensing has inspired a large number of research investigations. Scientists, biologists and engineers would like to understand the functional principles of the vibrissal sensing system from different aspects. Neuroscientists are trying to figure out how nerve impulses are processed from vibrissae to the brain and how an animal encodes the information. They perform laboratory experiments with living creatures, e.g. (Jadhav and Feldman 2010; Wolfe et al. 2008). Biologists usually describe the anatomy and morphology of vibrissae from species to species. They believe that the vibrissal sensing system played an important role during evolutionary development of mammals (Mitchinson et al. 2011).

For the engineers, the biological vibrissa gives an inspiration to design various artificial tactile sensors and find possible applications for them, as it promises to be competitive with artificial vision. Most often, the research focus lies on the

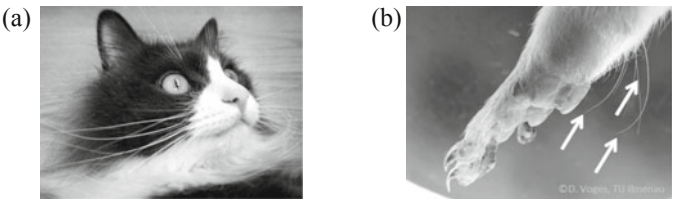

Fig. 1 **a** Mystacial and supraorbital vibrissae of a house cat; **b** Triple of carpal vibrissae at a forelimb of *Rattus norvegicus*, photo taken by Voges D (TU Ilmenau)

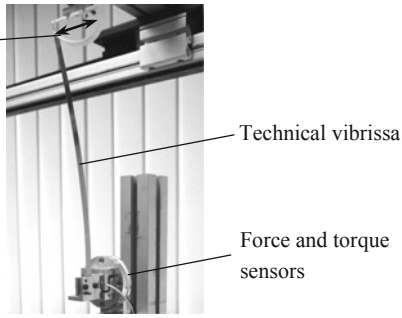

Fig. 2 The experimental setup at the Department of Mechanical Engineering (TU Ilmenau) for the quasi-static profile scanning

development of single sensors. Some interesting examples are the rotary actuated whisker for obstacle avoidance and the whisker-like sensor for underwater applications (Scholz and Rahn 2008; Valdivia y Alvarado et al. 2012). Furthermore, a variety of developed prototypes of mobile robots with a vibrissa-like sensory array can be found, e.g., in (Fend et al. 2004; Solomon and Hartmann 2006; Zimmer 1995). One of the latest platforms is the SCRATCHbot—a rat-like robot, which can move and position its whiskers toward specific objects with three degrees of freedom (Pearson et al. 2011).

Recent experimental investigations performed at the Department of Mechanical Engineering (TU Ilmenau) show that it is possible to reconstruct a profile of an object by one single quasi-static sweep of the straight technical vibrissa made of steel (Fig. 2). By measuring the clamping forces and the bending moment at the fixed base of the beam, the contact point with an object may be quantified. The theoretical analysis of the problem is based on the non-linear Euler–Bernoulli theory of the static deformable beam (Will et al. 2016).

Summarising the research on mathematical-mechanical modelling of vibrissae, two approaches may be marked out: rigid rod models, e.g. (Behn 2013; Berg and Kleinfeld 2003; Volkova et al. 2016a), and continuum elastic models, e.g. (Neimark et al. 2003; Scholz and Rahn 2008; Volkova et al. 2016b; Yan et al. 2013). The continuum models are in turn closer to the biological paradigm, as they take into account the inherent dynamical behaviour and the bending stiffness of the vibrissal hair. As for the modelling of the viscoelastic support of the hair inside the FSC, several spring and damping elements may be used, e.g. (Behn 2013). In (Volkova et al. 2016a), the FSC incorporating the blood capsule is modelled as a continuum volume filled with a viscous magnetic fluid. There, an approach to realise and control three-dimensional oscillations of the rigid rod is presented using an applied uniform magnetic field.

The present paper focuses on the non-linear process of the vibrissa sweeping across a surface of an object during texture discrimination. Frictional interactions between the tip of the vibrissal hair and a rough surface generate vibrations of the hair (Fig. 3). Since it has no receptors along the length, the tactile signals are transmitted by these mechanical vibrations to sensory receptors inside the FSC.

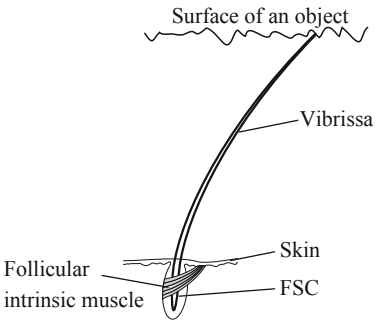

Fig. 3 Schematic drawing of a vibrissa sweeping past a rough surface

In this paper, the vibrissal hair is modelled as a straight elastic beam with linearly decreasing diameter along its length. The model describing in-plane vibrations of the beam stimulated by a periodic following force is developed. Based on asymptotic methods of mechanics, the *parametric resonance* of the beam is analysed theoretically. According to the so-called *resonance hypothesis* proposed in (Andermann and Moore 2008; Neimark et al. 2003), the vibrissa resonance may be a potentially useful mechanism during texture discrimination. It could amplify small tactile signals arising from the contact with an object and enchase the sensitivity of these biological tactile sensors. In the second part of the work, the numerical analysis of the problem using a finite element model is presented. The simulations are performed for various values of the excitation frequency of the applied force. The comparison of the theoretical and numerical results is made.

2 Theoretical Analysis

2.1 Geometry and Assumptions of the Model

Consider a truncated Euler–Bernoulli beam whose undeformed neutral axis is a straight line of a length L (Fig. 4). The radius $r(x)$ of the beam's circular cross-section evolves linearly along the axial direction:

$$r(x) = r_b - \frac{r_b - r_t}{L}x, \tag{1}$$

where r_b and r_t are, respectively, the radii at the base and the tip of the beam. The Cartesian coordinate system (x, y, z) is placed such that the x axis lies along the neutral axis of the beam, and the origin is in the middle of the base's cross-section. The Cartesian basis vectors are $\mathrm{e}_x, \mathrm{e}_y, \mathrm{e}_z$. The material properties of the beam are constant, i.e., the density ρ = const and the Young's modulus E = const. The support condition of the beam at the base is assumed to be pinned. It allows the beam to rotate around the z axis, but not to translate in any direction. At the end of the beam, the roller support is considered, which provides free rotation around the

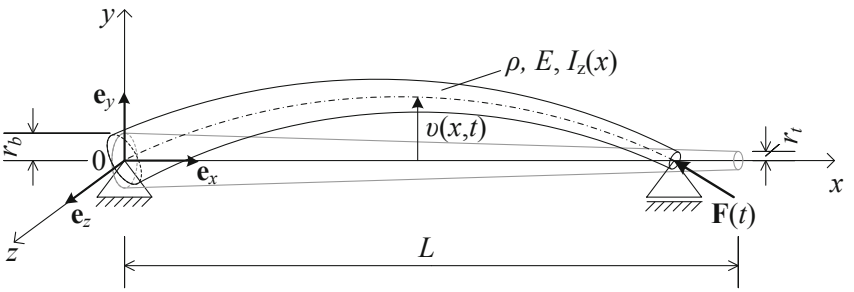

Fig. 4 Deflection of the straight truncated beam under the following force applied toward the cross-section at the tip

z axis and the horizontal deflection (Fig. 4). The beam is stimulated by a periodic force applied directly toward the cross-section of the beam at the tip:

$$\mathrm{F}(t) = -F_0 \cos(2\pi\,\Omega\, t)\mathrm{n}_t, \tag{2}$$

where F_0 is the amplitude, Ω is the excitation frequency, t is the time, and n_t is the normal to the cross-section at the tip. The assumed force $\mathrm{F}(t)$ corresponds to the frictional force, which arises from interactions between the vibrissal tip and the complex roughness profile of a surface (Fig. 3). Thus, it may be considered as a first harmonic component of the Fourier transform spectrum of the friction force.

It is supposed throughout that the transverse vibrations of the beam caused by the force $\mathrm{F}(t)$ about its straight natural configurations are in the x-y plane and *small*. The displacement vector of the axis points has the transverse component: $\mathrm{u}(x,t) = v(x,t)\mathrm{e}_y$.

2.2 Equation of Motion and Its Approximation

The small in-plain vibrational motion of the straight beam can be described with a single partial differential equation of the fourth order. With regard to the rotary inertia and in the absence of the force of viscous damping, the equation of motion in terms of $v(x,t)$ has the following form (Svetlitsky 2005; Zentner 2014):

$$m_0(x)\frac{\partial^2 v(x,t)}{\partial t^2} + \frac{\partial^2}{\partial x^2}\left(E\,I_z(x)\frac{\partial^2 v(x,t)}{\partial x^2}\right) + F_0\cos(2\pi\,\Omega\,t)\frac{\partial^2 v(x,t)}{\partial x^2} = 0. \tag{3}$$

Here, $m_0(x) = \pi\rho r^2(x)$ is the mass of the beam's element, and $I_z(x) = \pi\, r^4(x)/4$ is the moment of inertial of the cross-section.

The bending moment $\mathrm{M}(x,t) = M(x,t)\mathrm{e}_z$ at any cross-section of the beam can be expressed by the transverse displacement as:

$$M(x,t) = E\,I_z(x)\frac{\partial^2 v(x,t)}{\partial x^2}. \tag{4}$$

According to the chosen support combination, and since no external bending moment is applied, we have the following boundary conditions for the displacement function itself as well as for the second derivative of it:

$$v(0,t) = v(L,t) = 0, \quad \left.\frac{\partial^2 v(x,t)}{\partial x^2}\right|_{(0,t)} = \left.\frac{\partial^2 v(x,t)}{\partial x^2}\right|_{(L,t)} = 0. \tag{5}$$

In order to find the solution of the partial differential Eq. 3, let us first reduce it to an ordinary one using the Galerkin method (Kantorovich and Krylov 1958). We shall seek one-term approximate solution of Eq. 3 in the form:

$$v(x,t) = \sin\left(\frac{\pi x}{L}\right) f(t), \tag{6}$$

which satisfies the boundary conditions of the beam (Eq. 5). Substituting this expression in Eq. 3 with the requirement of the orthogonality of Eq. 3 to the function $\sin(\pi x/L)$, we obtain an ordinary second-order differential equation for the function $f(t)$. It can be written in the dimensionless form as:

$$\ddot{f}(\tau) + (1 - \varepsilon\cos(\gamma\,\tau))f(\tau) = 0. \tag{7}$$

Here, the dot notation is used to represent a time derivative of a function, and the dimensionless variables are introduced as follows:

$$\varepsilon = \frac{2\pi L^2 F_0}{b_1 E r_b^4},\ \gamma = \frac{\Omega}{\omega_1},\ \tau = 2\pi\,\omega_1 t,\ b_0 = \frac{1}{6}\left(1+\delta+\delta^2\right) - \frac{1}{4\pi^2}(1-\delta)^2 > 0, \tag{8}$$

$$b_1 = \frac{\pi^4}{10}\left(1+\delta+\delta^2+\delta^3+\delta^4\right) - \frac{\pi^2}{2}(1-\delta)\left(1-\delta^3\right) + \frac{3}{4}(1-\delta)^4 > 0,\ \delta = \frac{r_t}{r_b} \in [0,1].$$

The natural frequencies of transverse vibrations of the beam are (in Hz):

$$\omega_n = \frac{n^2 r_b}{4\pi L^2}\sqrt{\frac{b_1 E}{b_0 \rho}}, \quad n = 1,2,3,\ldots \tag{9}$$

In particular, for the cylindrical beam with constant radius $r(x) = r_b$, the assumed solution (Eq. 6) is an exact one. In this case, Eq. 3 reduces to the same Eq. 7 with the parameters $b_0 = 1/2$ and $b_1 = \pi^4/2$ as $\delta = 1$.

3 Parametric Resonance

Equation 7, known as the Mathieu equation, describes periodically excited vibrations of a system (McLachlan 1947). It has a cosinusoidal time-dependent coefficient of the term $f(\tau)$. The dimensionless parameters ε and γ, defined by Eq. 8, depend on parameters of the beam and the periodic applied force. It appears that for different values of ε and γ solutions of Eq. 7 may be periodic and bounded for all time, or the amplitude of the vibrations in solutions may grow progressively in time (*parametrical resonance*). Let us determine analytically and numerically ranges of the parameters, when the parametric resonance of the beam takes place.

3.1 Procedure of Averaging

For the approximate analysis of the oscillating process described by Eq. 7, the method of averaging is used (Bogolyubov and Mitropoliskii 1961). First, in order to reduce Eq. 7 to the standard form, it is assumed that the function $f(\tau)$ and its derivative have the form: $f(\tau) = a(\tau)\cos(\psi(\tau))$ and $\dot{f}(\tau) = -a(\tau)\sin(\psi(\tau))$.

Then, the differential equation of the second order (Eq. 7) converts to the system of two equations of the first order for the new variables $a(\tau)$ and $\psi(\tau)$:

$$\dot{a}(\tau) = -\frac{\varepsilon}{2}a(\tau)\sin(2\psi(\tau))\cos(\gamma\tau), \quad \dot{\psi}(\tau) = 1 - \varepsilon\cos^2(\psi(\tau))\cos(\gamma\tau). \tag{10}$$

As it will be shown, the most intense parametric resonance occurs for values of the excitation frequency Ω close to $2\omega_1$ of free vibrations of the beam. Therefore, we can set $\gamma = 2 + \varepsilon\Delta$, where Δ corresponds to the amplification factor of the parametric excitation. Consider the amplitude F_0 to be small in comparison with the elastic forces of the beam element, so that ε can be treated as a small positive parameter: $0 < \varepsilon \ll 1$. If $a(\tau)$ and $\xi(\tau) = \gamma\tau - 2\psi(\tau)$ are smooth functions of the time such that their derivatives are small terms of order ε, the values of these functions can be seen as the superposition of slowly varying part and small rapidly oscillating terms. Thus, they can be averaged on ψ over one period:

$$\dot{a}_0(\tau) = \frac{1}{2\pi}\int_0^{2\pi} \dot{a}(\tau)d\psi = \frac{\varepsilon}{4}a_0(\tau)\sin(\xi_0(\tau)), \tag{11}$$

$$\dot{\xi}_0(\tau) = \frac{1}{2\pi}\int_0^{2\pi} \dot{\xi}(\tau)\,d\psi = \varepsilon\Delta + \frac{\varepsilon}{2}\cos(\xi_0(\tau)).$$

3.2 Region of the Principal Parametric Resonance

The non-linear system (Eq. 11) may be simplified to a linear one with constant coefficients by defining new variables $\eta(\tau) = a_0(\tau)\cos(\xi_0(\tau)/2 + \pi/4)$ and $\varsigma(\tau) = -a_0(\tau)\sin(\xi_0(\tau)/2 + \pi/4)$:

$$\dot{\eta}(\tau) = -\frac{\varepsilon}{4}\eta(\tau) + \frac{\varepsilon\Delta}{2}\varsigma(\tau). \quad \dot{\varsigma}(\tau) = -\frac{\varepsilon\Delta}{2}\eta(\tau) + \frac{\varepsilon}{4}\varsigma(\tau). \tag{12}$$

The matrix corresponding to the system (Eq. 12) has the following eigenvalues:

$$\lambda^2 = \frac{\varepsilon^2}{4}\left(\frac{1}{4} - \Delta^2\right). \tag{13}$$

Thus, the solution of Eq. 12 is aperiodic and unstable, when there is an eigenvalue with positive real part, i.e., for $|\Delta| < 1/2$ around the dimensionless frequency value $\Omega/\omega_1 = 2$. This means that the resonance takes place within the interval

$$0 < \varepsilon \ll 1 \quad \text{and} \quad 2 - \frac{\varepsilon}{2} < \frac{\Omega}{\omega_1} < 2 + \frac{\varepsilon}{2}. \tag{14}$$

It is called the *region of the principal parametric resonance*. The width of this range is proportional to the parameter ε.

Other frequency ranges of the parametric resonance are close to the values $\Omega = 2\omega_1/n$ for any natural number n (Landau and Lifshitz 1969). However, the width of them gets narrow proportionally to the value ε^n as n increases. In practice, the cases for n = 1, 2, and 3 (rarely) are usually observed.

4 Numerical Analysis and Results

The small transverse vibrations of the parametrically excited beam are described by the partial differential Eq. 3. The solution of it with respect to the boundary conditions (Eq. 5) may be obtained by means of the finite element method. The numerical simulations are performed using software ANSYS Workbench 16.2.

Two particular models of the beam are considered:

1. A straight cylindrical beam (CB) with a constant radius of the cross-section.
2. A straight truncated beam (TB), when the radius at the tip is half of that at the base: $r_t = r_b/2$.

Table 1 Values of the parameters used in numerical simulations

Parameters	Cylindrical beam (CB)		Truncated beam (TB)
	Line body	Solid cylinder	Solid body
Length L (mm)	50	1	50
Radius r_b (mm)	1	–	1
Radius r_t (mm)	1	1	0.5
Density ρ (kg m^{-3})	1000	10^{-6}	1000
Young's modulus E (Pa)	10,313	2×10^{13}	10,313

4.1 Remarks on the Simulations

For both beam models, the vibrational characteristics (natural frequencies and mode shapes) are evaluated using an analysis system ANSYS "Modal". The dynamic response of a structure under the action of a periodic following load is calculated within the ANSYS module "Transient structural".

The CB is modelled as a line body with a thin circular solid cylinder attached at the right end. The latter one is needed to apply the periodic following force perpendicular to the cross-section. The cylinder may be considered massless and rigid. The transition between beam elements (beam 188, 50 elements) of the line body and solid elements (solid 186, 16 elements) of the cylinder is defined with the multi-point constraint bonded contact. Both translational and rotational degrees of freedom are accounted for. The TB is modelled as a whole using solid elements (solid 186, 504 elements). The values of the parameters for both models are given in Table 1. The boundary conditions are applied according to the theoretical formulation of the problem. Within the simulations, no damping is considered. The numerical damping is defined manually to be zero.

For the chosen parameter sets, the natural frequencies are listed in Table 2. It is shown that the values of the CB obtained numerically for three different meshing elements coincide with the theoretical eigenfrequencies given by Eq. 9. It has to be noted that the values of the parameters assigned to the beam (Table 1) do not correspond to vibrissae values reported in literature, e.g. (Neimark et al. 2003; Voges et al. 2012). They are chosen in such a way that $\omega_1 \approx 1$ Hz of the CB. This in turn further allows using a reasonable adequate time step size (10^{-2}–10^{-3} s) in transient simulations. The theoretical natural frequencies of the TB give upper boundary values, i.e., they are slightly higher than the numerical results (Table 2).

The transient analysis of parametric vibrations requires an initial deflection of the beam from the equilibrium position. Thus, the load process is developed in three steps: (1) [0, 0.25] s, (2) [0.25, 0.5] s, and (3) [0.5, 30] s. Within the first two steps, the impulse force is applied and discharged linearly at the midst of the beam in the transverse direction. Its maximum magnitude is 10–7 N. Then, within a time range [0.25, 30] s, the main load is applied as a pressure $P(t) = -P_0 \cos(2\pi\,\Omega\, t)$, $P_0 = 3$ Pa, normal to the cross-section at the right end.

Table 2 Natural frequencies of transverse vibrations of the CB and TB

Frequency(Hz)	Cylindrical beam (CB)				Truncated beam (TB)	
	Theory	Numerical simulations (ANSYS)			Theory	ANSYS
	Equation 9	Beam 3	Beam 188	Solid 186	Equation 9	Solid 186
ω_1	1.0089	1.007	1.0068	1.0053	0.7835	0.709
ω_2	4.0355	4.008	4.007	4.0016	3.1338	2.9593
ω_3	9.08	8.9526	8.9439	8.9324	7.0511	6.6026
Elements		50 + 16	50 + 16	512		504
Nodes		101 + 93	101 + 93	2201		2167

Table 3 Regions of the parametric resonance of the CB and TB (in Hz)

	Theory	Numerical simulations (ANSYS)
Region of the principal parametric resonance: $\Omega \approx 2\omega_1$		
CB	$1.8691 < \Omega < 2.1665$	$1.87 \leq \Omega \leq 2.15$
TB	$1.483 < \Omega < 1.6508$	$1.32 \leq \Omega \leq 1.50$
Second range of the parametric resonance: $\Omega \approx x_1$		
CB	$0.9907 < \Omega < 1.0125$	$0.99 \leq \Omega \leq 1.01$

4.2 Regions of the Parametric Resonance

The dynamic response of the system under the parametric excitation is simulated for various frequency values. For the CB, the solution is found to be unstable for the frequencies close to the doubled eigenfrequency of the beam (region of the principal parametric resonance), as well as for the frequencies around this value (second range of the parametric resonance). For the TB, the region of the principal parametric resonance is obtained. Within these frequency intervals, the vibrations of the beam are unstable, i.e., their amplitude increases exponentially with time.

The comparison of the theoretical (Eq. 14) and numerical regions of the parametric resonance is given in Table 3. It may be seen that the results of the CB correspond to each other. Moreover, it is shown that the response of the system on the parametric excitation is qualitatively stronger within the region of the principal parametric resonance than within the second range. For the TB, a slight discrepancy between the theoretical and numerical results is observed. It is associated with the accounting of the variable radius of the cross-section.

In Fig. 5, some simulation results of the CB and TB are presented. The averaged amplitude of the theoretical solution is plotted for comparison as a dash line.

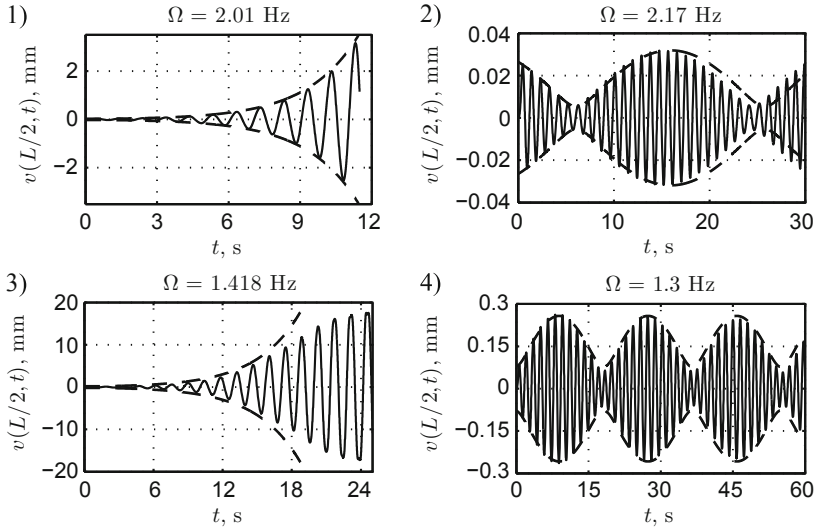

Fig. 5 Transverse displacement of the CB (**a**, **b**) and the TB (**c**, **d**): **a**, **c** unstable solution of the principle parametric resonance; **b**, **d** steady-state solution; — numerical simulations; – – the theoretical averaged amplitude $a_0(t)$ for: **a** $a_0(0) = 0.024$ mm, $\psi(0) = 0$; **b** $a_0(0) = 0.0265$ mm and $\psi(0) = 1.4573$; **c** $a_0(0) = 0.18$ mm, $\psi(0) = 0$, $\Omega = 2\omega_1 = 1.5669$ Hz; **d** $a_0(0) = 0.078$ mm, $\psi(0) = 1.7453$, $\Omega = 1.461$ Hz

5 Conclusions

In this work, a model of a straight truncated beam is developed to study the vibrational motion of mammal's vibrissae. The transverse oscillations of the beam stimulated by a periodic following force are investigated theoretically and numerically. It is shown that the parametric resonance of the beam occurs at the specific ranges of the excitation frequency, within which the vibrations of the beam are unstable with exponentially increasing amplitude. Together with the realisation of the viscoelastic support of an artificial tactile sensor, it may be a potentially useful method for amplifying small signals arising from the contact with an object. Future investigations will also focus on the design of sensor arrays consisting of several vibrissa elements.

Acknowledgments The work was supported by the Deutsche Forschungsgemeinschaft (DFG) within the Grant ZI 540-16/2.

References

Andermann M, Moore C (2008) Mechanical resonance enhances the sensitivity of the vibrissa sensory system to near-threshold stimuli. Brain Res 1235:74–81

Behn C (2013) Mathematical modeling and control of biologically inspired uncertain motion systems with adaptive features. Habilitation thesis, TU Ilmenau

Berg R, Kleinfeld D (2003) Rhythmic whisking by rat: retraction as well as protraction of the vibrissae is under active muscular control. J Neurophysiol 89:104–117
Bogolyubov N, Mitropoliskii Y (1961) Asymptotic methods in the theory of nonlinear oscillations. Gordon and Breach Science Publishers, New York
Dehnhardt G, Kaminski A (1995) Sensitivity of the mystacial vibrissae of harbour seals (Phoca vitulina) for size differences of actively touched objects. J Exp Biol 198:2317–2323
Dörfl J (1982) The musculature of the mystacial vibrissae of the white mouse. J Anat 135:147–154
Ebara S, Kumamoto K, Matsuura T et al (2002) Similarities and differences in the innervation of mystacial vibrissal follicle-sinus complexes in the rat and cat: a confocal microscopic study. J Comp Neurol 449:103–119
Fend M, Bovet S, Hafner VV (2004) The artificial mouse—a robot with whiskers and vision. In: Proceedings of the 35th international symposium on robotics, Paris, 23–26 Mar 2004
Jadhav SP, Feldman DE (2010) Texture coding in the whisker system. Curr Opin Neurobiol 20 (3):313–318
Kantorovich L, Krylov V (1958) Approximate methods of higher analysis. P. Noordhoff, Groningen
Landau L, Lifshitz E (1969) Mechanics. Course of theoretical physics. Pergamon Press, Oxford
McLachlan NW (1947) Theory and application of Mathieu functions. Clarendon Press, Oxford
Mitchinson B, Grant RA, Arkley K et al (2011) Active vibrissal sensing in rodents and marsupials. Phil Trans R Soc B 366:3037–3048
Neimark M, Andermann M, Hopfeld J et al (2003) Vibrissa resonance as a transduction mechanism for tactile encoding. J Neurosci 23:6499–6509
Niederschuh S, Witte H, Schmidt M (2014) The role of vibrissal sensing in forelimb position control during travelling locomotion in the rat (Rattus norvegicus, Rodentia). J Zool 118 (1):51–62
Pearson MJ, Mitchinson B, Sullivan JC et al (2011) Biomimetic vibrissal sensing for robots. Phil Trans R Soc B 366:3085–3096
Scholz G, Rahn C (2008) Profile sensing with an actuated whisker. IEEE T Robot Autom 20:124–127
Solomon JH, Hartmann MJ (2006) Biomechanics: robotic whiskers used to sense features. Nature 443(7111):525
Svetlitsky V (2005) Dynamics of rods. Springer, Berlin
Valdivia y Alvarado P, Subramaniam V, Triantafyllou M (2012) Design of a bio-inspired whisker sensor for underwater applications. In: IEEE sensors 2012, Taipei, 28–31 Oct 2012, pp 92
Vincent S (1912) The function of vibrissae in the behavior of the white rat. Behav Monogr 1:1–81
Voges D, Carl K, Klauer G et al (2012) Structural characterization of the whisker system of the rat. IEEE Sens 12(2):332–339
Volkova T, Zeidis I, Naletova VA et al (2016a) The dynamical behavior of a spherical pendulum in a ferrofluid volume influenced by a magnetic force. Arch Appl Mech (First online)
Volkova T, Zeidis I, Witte H et al (2016b) Analysis of the vibrissa parametric resonance causing a signal amplification during whisking behaviour. J Bionic Eng 13:312–323
Will C, Steigenberger J, Behn C (2016) Bio-inspired technical vibrissae for quasi-static profile scanning. Lect Notes Electr Eng (LNEE) 370:277–295
Wolfe J, Hill DN, Pahlavan S et al (2008) Texture coding in the rat whisker system: slip-stick versus differential resonance. PLoS Biol 6:e215
Yan W, Kan Q, Kergrene K et al (2013) A truncated conical beam model for analysis of the vibration of rat whiskers. J Biomech 46:1987–1995
Zentner L (2014) Nachgiebige Mechanismen. De Gruyter Oldenbourg, München
Zimmer U (1995) Self-localization in dynamic environments. In: IEEE/SOFT international workshop BIES'95, Tokio, 30–31 May 1995, p 8